Mechanical Systems and Signal Processing 36 (2013) 604–617

Contents lists available at SciVerse ScienceDirect

Mechanical Systems and Signal Processing

journal homepage: www.elsevier.com/locate/ymssp

Development and testing of a dynamic absorber with corrugated piezoelectric spring for vibration control and energy harvesting applications

R.L. Harne *

Department of Mechanical Engineering, University of Michigan, 2350 Hayward St., 2250 G.G. Brown Building, Ann Arbor, MI 48109-2125, USA

ARTICLE INFO

Article history:
Received 19 August 2012
Accepted 16 October 2012
Available online 21 November 2012

Keywords:
Vibration control
Energy harvesting
Structural dynamics
Piezoelectricity

ABSTRACT

Vibrational energy harvesting devices are often designed in a manner analogous to classical dynamic vibration absorbers (DVAs). An electromechanical mass–spring system is devised so as to resonate at the frequency most dominant in the environmental vibration spectrum; the consequent device oscillation is converted to a electrical signal which is harnessed for immediate usage or as a charging mechanism for a battery. The DVA is likewise designed but with the intention of inducing substantial inertial influence upon a host structure for vibration control purposes, either to globally dampen the vibration of the main body or, in an undamped configuration to "absorb" the primary system vibration at a single frequency. This paper describes the development of an electromechanical mass–spring–damper which seeks to serve both goals of passive vibration control and energy harvesting. The device utilizes a piezoelectric film spring and a distributed mass layer so as to be suitable for the attenuation of surface vibrations and to convert a portion of the absorbed energy into electric power. The development and design of the device are presented and the results of realistic tests are provided to show both the potentials and the challenges encountered when attempting to superpose the goals of vibration control and energy harvesting.

1. Introduction

Much research has been conducted to convert ambient vibrational energy into electrical power with a general aim to reduce or eliminate the reliance on disposable power sources in remote environments or for self-powered MEMS [1–4]. Resonant devices are designed such that they have a natural frequency equal to the frequency of vibration most prominent in the host structure [5–8]. The damping induced upon the structure via energy harvesting is itself well-known from the perspective of a first-order dissipative influence between the electrical and mechanical domains [9–14]. This is recognized to be a consistent effect for most energy harvesting platforms (*e.g.* piezoelectric, electromagnetic, etc.) such that in some cases the analyses have been conducted assuming that the consequence of electromechanical coupling may be simplified to an equivalent damping term in a mechanical governing equation [1,15,16]. This approach is known to present an incomplete picture for energy harvesting studies when the coupling strength is moderate to great [8,14,17] but does provide a straightforward and intuitive understanding of the fundamental electromechanical influences.

* Tel.: +1 7346158747.
E-mail address: rharne@umich.edu

0888-3270/$ - see front matter © 2012 Elsevier Ltd. All rights reserved.
http://dx.doi.org/10.1016/j.ymssp.2012.10.012

Many energy harvesting studies assume that the harvester is excited by an infinite resource of energy in the form of base excitation or applied forces [1,2,7,8,15,16]. In the event that the harvester becomes more inertially substantial relative to the greater vibrating structure, different analyses must be applied. This perspective is also exemplified in the study of multi-modal harvesters [18–21] or multi-mass harvesters [22,23] in which case the degrees-of-freedom (DOF) of the harvester themselves dynamically interact. Given the analogy between a DVA and energy harvester, this larger view of the excited host vibrating structure and attached harvester brings to light the potential for concurrent vibration control and energy harvesting. Thus, the study becomes a dual-objective approach whereby the electromechanical device is both a passive vibration control implement and power harvesting device. Studies have recently considered this perspective as a multi-objective optimization problem [24] and have probed for insight into how one goal may be achieved relative to the other [25].

It is this perspective which the present work adopts. The focus application of the study is on the vibrations of structural panels which are oftentimes a source of undesirable radiated noise. The panels may be excited via a number of means (structural–acoustic coupling, direct forces, traveling waves through a frame, etc.), yielding a vibration spectrum regularly dominant at frequencies less than 200 Hz. In order to suppress such vibrations, numerous passive treatment designs have been considered including constrained-layer damping [26,27], arrays of discrete mass–spring systems [28–31], and continuously distributed spring–mass layers [32–34]. In contrast to merely dissipating the energy mechanically, this paper presents the design and development of a distributed electromechanical device capable of practical vibration control and energy conversion for power harvesting applications.

The design of the energy harvesting vibration absorber (EHVA) is here presented. The configuration implements a corrugated piezoelectric film (PVDF) spring in conjunction with a distributed mass layer. The development of the PVDF spring is provided in detail to justify its final design. Initial laboratory shaker tests are presented that show the fundamental mass–spring dynamics and indicate some difficulties in the current manufacture of the device. Two tests using sample EHVAs are presented to highlight practical issues involved in simultaneous passive vibration control and energy harvesting with recommendations for future investigation and means by which to evaluate both objectives concurrently.

2. EHVA design

2.1. Related concepts and design selection

An objective of this work is to develop a device suitable for the passive attention of surface vibration. Given the distributed nature of the primary, excited system, it is logical to pursue a solution which will be distributed over the surface of the host structure. This is the framework which the present study adopts and is like-minded with other research that have considered distributions of oscillators [28–31] or continuously distributed devices [32–34] for surface vibration control.

From a one-dimensional perspective, the cantilevered piezoelectric beam harvester employs a piezoelectric spring with an inertial mass. This is also the classical vibration absorber construction. However, a cantilevered beam induces moments upon a host structure. While a reactive moment working on a vibrating structural panel may be useful in suppressing vibration—and it is duly noted that this *is* in fact the basis for much piezoelectric patch shunt damping or active control research [12,13,35,36]—substantial forces would be more practical if a suitable design may be devised to yield a distributed force over the vibrating surface. Thus, a design was pursued which would utilize the dynamic concept of the DVA for a distributed platform while also using available electromechanical elements to convert the strain energy to an electrical signal for energy harvesting. Therefore, as opposed to the development of a second-order electrical suppression effect in the style of resonant-shunt piezoelectric devices [10,12,37], the present study aims to develop a second-order mechanical effect while still employing an electromechanical mechanism.

Some devices may be found in the literature for active structural and/or noise control which utilize piezoelectric elements not directly attached to the vibrating structure, but instead embedded within the device itself. Smart foam is one such device, consisting of an activated PVDF film curvature within a poroelastic material for both passive and active vibration and noise control purposes [38–41]. Other studies have considered this same configuration but have added a distributed top mass layer [42], such that in tandem with the poroelastic foam, the full device exhibits a rigid-body motion natural frequency, as the mass compresses the foam spring beneath it. Used passively, the embedded PVDF film within the poroelastic material may an energy harvesting implement as it is strained during compression of the foam spring. However, the low concentration of film (and use of PVDF itself which has low electromechanical coupling) was recently found to yield marginal electrical output from analytical investigation [34].

If employing PVDF film as the energy conversion mechanism, despite its advantageous low-cost relative to other piezoelectric materials, it must be used in sufficient concentration within the spring design so as to provide a viable net electrical signal. An active PVDF film spring curvature was earlier patented [43] and later used with a mass layer for the similar aim of active and passive vibration control purposes [32]. In this configuration, a sinusoidally or circularly corrugated PVDF film is attached to a distributed mass layer; as opposed to the spring being embedded within a greater medium, the corrugated PVDF spring fully supports the mass layer and as such has greater active control authority given the concentration of PVDF material. Fig. 1 shows a cross-section of this design ultimately employed in the present work.

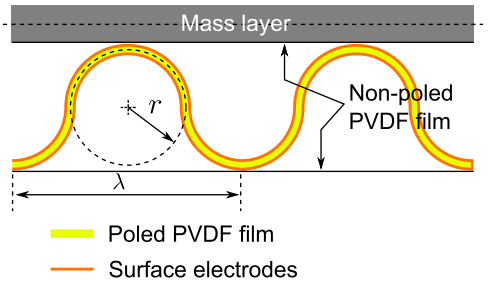

Fig. 1. Cross-section of the device with a distributed mass layer and distributed spring layer (corrugated piezoelectric film) bounded by two non-poled PVDF sheets.

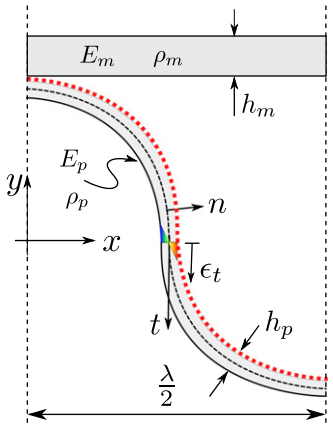

Fig. 2. FE model geometry indicating tangential strain component, ϵ_t, to be computed along the PVDF film arc length. (For interpretation of the references to color in this figure caption, the reader is referred to the web version of this article.)

A distributed mass layer is adhered to a circularly corrugated PVDF spring layer, the latter being constrained to its form by thin lines of epoxy to two non-poled PVDF film sheets.

As the mass compresses the PVDF spring beneath it when the device vibrates in a single degree-of-freedom (SDOF) resonance, it may be logical to presume that the bending strain induced along the film curvature would change sign at certain locations: strain nodes. These features have been shown to be an important consideration in multi-modal piezoelectric beam energy harvesting, namely that etching of the surface electrodes and recombination of the separate signals out-of-phase is necessary in order to avoid electrical output cancelation [44]. As a result it was imperative to evaluate where strain nodes may exist along the wavelength, λ, of the present PVDF film spring such that the electrode surfaces may be appropriately etched.

2.2. Strain node investigation

Finite element (FE) analysis was employed to determine strain node locations as the EHVA vibrates in SDOF resonance. A half-cross-section model of typical geometry was developed using the COMSOL software package [45] with an eigenvalue solver. A schematic of the model geometry is shown in Fig. 2. For this structural analysis, the necessary input parameters were Young's modulus, E, density, ρ, and thickness h, for the piezoelectric and mass layers, using subscripts p and m, respectively. As the strain along the piezoelectric film surface is of interest, the surface tangential strain, ϵ_t, was computed along the electrode half-wavelength, denoted as the red dotted line in Fig. 2, from the Cartesian strain components, ϵ_x and ϵ_y, as

$$\epsilon_t = \epsilon_x|\cos\theta| + \epsilon_y|\sin\theta|, \quad 0 \le \theta \le \pi \tag{1}$$

where $\theta = \pi/2$ indicates the center point along the arc length depicted in Fig. 2. In the FE model, symmetric boundary conditions were used for both planes $x=0$ and $x=\lambda/2$ and the bottom point of the PVDF film at $x=\lambda/2$ was kept fixed. Thus, the first eigensolution of this model corresponds to the SDOF rigid-body resonance dynamic. Geometric and material parameters used in the model are given in Table 1. A fine mesh was selected and further mesh refinement showed no improvement in the predictions, providing assurance for proper convergence.

Fig. 3 plots a deformed surface plot of the FE model results for the first eigenmode, indicating the shape of the device cross-section at one half-cycle through the SDOF resonance dynamic. The surface contour represents the tangential strain

Table 1
Geometric and material properties for FE simulation.

E_m (GPa)	ρ_m (kg m^{-3})	h_m (mm)	E_p (GPa)	ρ_p (kg m^{-3})	h_p (mm)	λ (mm)
200	7850	1	2.9	1780	0.1	20

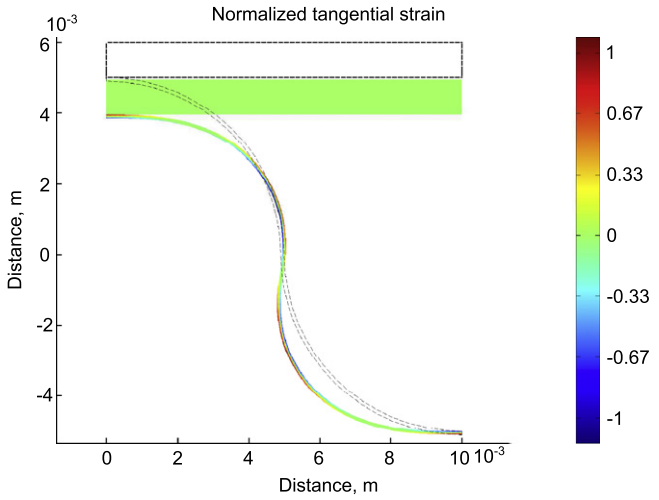

Fig. 3. FE model output of normalized tangential strain showing deformed shaped of device cross-section at one half-cycle of SDOF resonance.

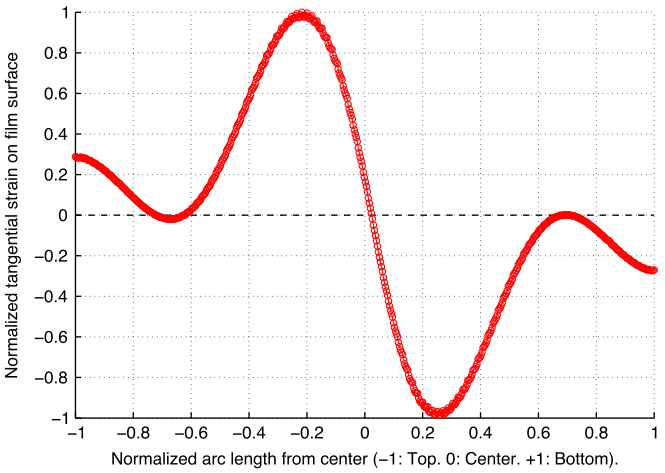

Fig. 4. Normalized tangential strain on top film surface.

computed everywhere over the film section, normalized to the maximum value. The SDOF rigid-body motion of the device is evident from the deformed section shape, as the mass layer moves rigidly and compresses the corrugated film beneath it, inducing a bending surface strain along the PVDF film. It is this strain on the top and bottom film surfaces which is of importance, as these are the locations of the electrodes which cover the film for charge extraction or activation.

Fig. 4 plots the normalized tangential strain of the top PVDF film surface (dashed red line in Fig. 2 schematic) along the arc length of the sample, from the top (indicated as -1 on the x-axis) to the bottom ($+1$ on the x-axis). Intuitively, there is a strain node, $\epsilon_t = 0$, located near to the center along the arc length. Additionally, there are two strain nodes at approximately ± 0.7 along the normalized arc length from center. However, these strain nodes do not yield a change in sign of the tangential surface strain. They are the result of the change in influence of the vector components of ϵ_t as the regions of the arc length < -0.7 and > 0.7 are dominated by ϵ_x while the center portion > -0.7 to < 0.7 is dominated by ϵ_y. Since the tangential strain changes sign only at the approximate center along the arc length, the electrode surface need only be etched at these locations.

3. Experimental sample construction

As the FE model considered just one half-wavelength of the device cross-section, this indicates that the corrugated PVDF spring must be etched twice per wavelength, on the top and bottom film surfaces, at approximately the center position of the arc length (thus, four etches per wavelength). Fig. 5 depicts the etched film construction for a multitude of corrugations. While the etched locations occur every $\lambda/2$ from the perspective of the cross-section after corrugation, the PVDF film must naturally be etched prior to corrugation in which case the etch-to-etch distance is $\pi\lambda/4$ due to the final circular corrugation shape.

All the samples considered in this work were constructed by the author and great care was taken to as accurately as possible reproduce this etching distance along the length of the many corrugations. In the present study, etching was undertaken by hand using an exceptionally fine watercolor brush and ferric chloride solution, but the author recognizes that such etching techniques are performed in industries such as circuit board manufacture. Thus, while it was difficult in practice to construct experimental samples of absolute regularity, there are practical industrial-scale solutions to maintaining consistent etching and construction for the present EHVA design.

The etched PVDF film was held in place to the non-poled PVDF film sheets via very thin lines of quick-drying epoxy. These distributed piezoelectric spring samples were allowed to cure for several days after which a top mass layer was bonded via a thin layer of epoxy to one of the non-poled PVDF film sheets, thus completing the final sample. Only after several additional days of curing the samples were employed for testing. Immediately prior to being implemented in tests, electrode leads were attached with copper conductive adhesive and further secured using masking tape. Fig. 6(a) shows a photograph of one small sample used for shaker testing and Fig. 6(b) shows a close-up of the etched and corrugated PVDF film spring.

4. Experimental SDOF response via shaker testing

Several samples were constructed using identical design parameters as given in Table 2. A total of 6 wavelengths of the corrugated PVDF film were used and the top mass layer did not extend beyond this span. The EHVA depth was 50 mm. Tests were conducted using a modal shaker platform to excite the sample in purely SDOF response and the measurements taken were of the platform acceleration (accelerometer), the top mass velocity (laser vibrometer), and electrical voltage output from the etched electrode leads as measured across an external load resistance kept constant at 560 kΩ. From these

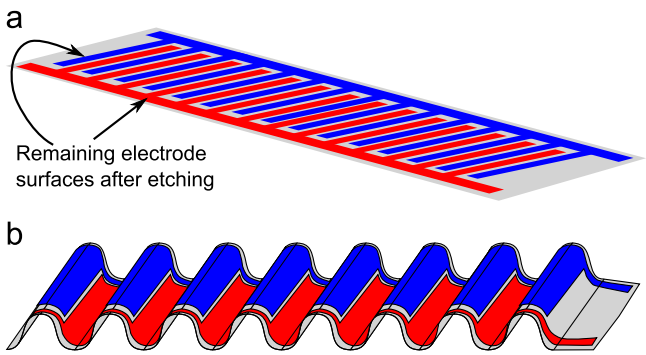

Fig. 5. PVDF film surface after etching and (a) before corrugation and (b) after corrugation.

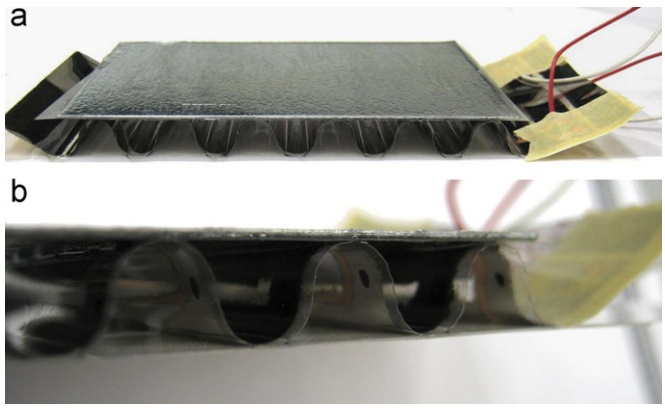

Fig. 6. Complete EHVA sample. (a) Full device. (b) Zoom of etched electrode surfaces.

Table 2
Geometric and material properties for shaker test samples.

E_m (GPa)	ρ_m (kg m^{-3})	h_m (mm)	E_p (GPa)	ρ_p (kg m^{-3})	h_p (mm)	λ (mm)
200	7850	1	2.9	1780	0.0286	12.7

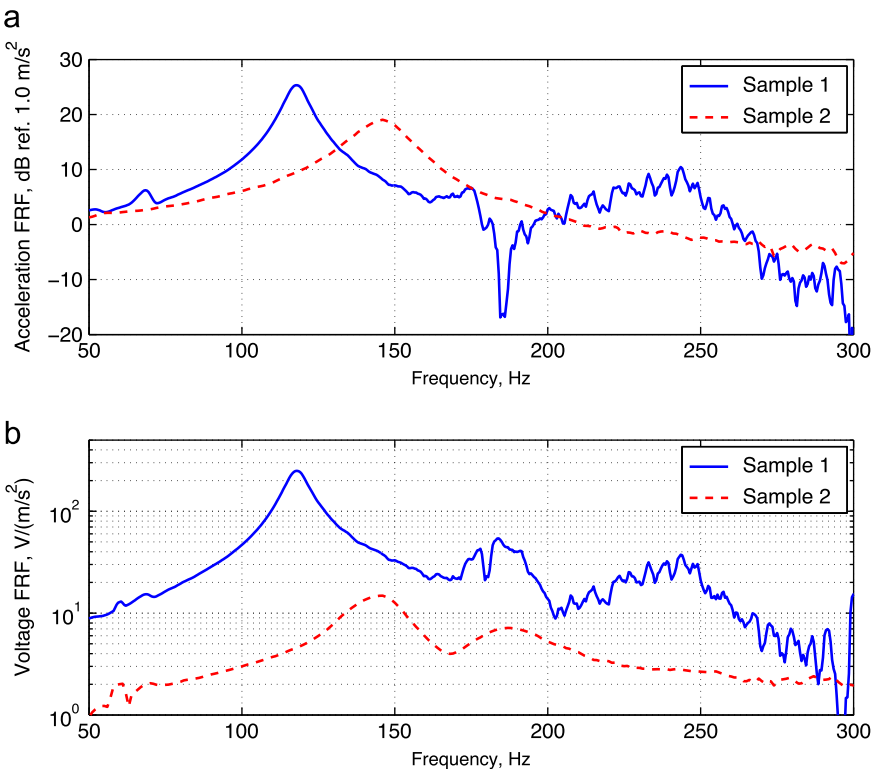

Fig. 7. Comparison of two identical experimental sample (a) acceleration FRFs and (b) voltage FRFs. The substantial deviation in the responses was concluded to be the result of the epoxy bonds between the corrugated and bounding PVDF film sheets.

measurements were computed the acceleration FRF of the top mass acceleration to the input acceleration and the voltage FRF of the output voltage to the input acceleration. The top mass acceleration was determined by taking the derivative of the top mass velocity measurements.

Fig. 7 plots the acceleration FRF and voltage FRF for two such samples. Despite being constructed using an identical parameter design, a substantial difference in the sample stiffness and damping is indicated by the location and magnitude of the SDOF resonance frequency. After considerable experience of producing the parts by hand, the discrepancies from part-to-part were deemed to be the result of the epoxy bonds between the corrugated film and the bounding non-poled PVDF sheets. Using too much epoxy was found to ironically both stiffen and dampen the samples: the prior because there was reduced distance from joint-to-joint thus making the transverse deflection less flexible and the latter because the epoxy is inherently a dissipative polymer once cured. Thus, for sample 2 in Fig. 7, it is anticipated that an increase in epoxy was ultimately the cause for such a large increase in the SDOF resonance frequency from sample 1, as well as the damping increase which is seen to adversely affect the voltage response in Fig. 7(b).

Curve-fitting both plots with 2nd-order polynomials from whose roots may be determined the loss factor of the sample shows that sample 1 has an equivalent loss factor of 5.5% while sample 2 has a loss factor of 11.7%. As a result of iterative investigations in constructing the samples and determining the consistency of part-to-part mechanical and electrical output, it was determined that the epoxy was an unfortunately influential and necessary component in the present design. Great care was thereafter taken to use as little epoxy as possible while still manufacturing parts capable of amply constraining the corrugated PVDF film spring.

Lastly, the dynamic responses of sample 1 in Fig. 7 around 240 Hz were known to be the result of rigid-body rotation of the top mass [46]; this same feature was observed for sample 2 but at a frequency greater than those shown in Fig. 7. This effect is unavoidable in practice when applying EHVAs to modally vibrating surfaces but is not observed to adversely affect the harvested output or vibration control capability of the device near to its SDOF resonance. So long as the EHVAs were positioned on an antinode of the surface modal vibration having an eigenfrequency equal to the SDOF resonance frequency

of the EHVA, the harvesters were observed to perform as designed in suppressing the host structure vibration and converting a portion of the energy into electrical power.

5. Laboratory test: EHVA on a panel

Following shaker testing to confirm the anticipated fundamental mechanical and electrical dynamics of the EHVAs, several further samples were produced to be used for testing on a vibrating surface, namely an aircraft-grade structural panel. A test panel was constructed of aluminum and mounted on thin shims to closely replicate classical simple support boundary conditions. A shaker, short stinger and force transducer were attached to the panel center to excite the panel with white noise from 50–200 Hz. On the opposite side of the panel, an accelerometer was placed at the panel center at the location of the stinger and force transducer mounting bolt, as indicated in Fig. 8. The (1,1) mode of the panel was measured to be 89.5 Hz and the accelerance transfer function (TF) was computed as the transfer function between the accelerometer output and the input force. Only the lowest structural mode was of interest in the present study given that most ambient vibration for energy harvesting applications is likely to result from the deflection of a structure in its fundamental mode.

The EHVA was designed so as to exhibit a SDOF transverse natural frequency of 94 Hz, near to the natural frequency of the panel (1,1) mode (material selection and the concerns of epoxy made it difficult to exactly achieve a SDOF resonance of 89.5 Hz and thus 94 Hz was deemed admissible for testing). The EHVA was thereafter placed as close to panel center as possible (shown in Fig. 8) secured with a thin adhesive layer. The accelerance between the input force and the panel center acceleration was again computed for a variety of load resistances, R_1, attached to the EHVA electrodes combined out-of-phase. The EHVA constituted an additional 1% of mass to the panel or, alternatively, a mass ratio of $\mu = 0.0102$.

The panel response before and after application of the EHVA is plotted in Fig. 9 for several selections of load resistance of R_1. Like a classical one-dimensional (1D) vibration absorber, the EHVA significantly attenuates the panel (1,1) mode; greater than 15 dB of mechanical attenuation is observed. Two split resonances are induced by the device: 79 and 104 Hz. This effect is characteristic of traditional vibration absorbers [47] indicating a similarity between the present distributed EHVA design for structures and point mass–spring–dampers for 1D mechanical systems.

As the load resistance R_1 is modified additional dynamic influence is induced by the EHVA. A minor shunt damping effect and increase in the higher split resonance frequency are observed as R_1 increases. No further damping or increase in the split resonance frequency was observed for larger values of R_1 than 820 kΩ, nor was any change observed for smaller R_1 than the panel response shown for $R_1 = 150$ kΩ. The shunt damping effect is that which has been observed in prior work

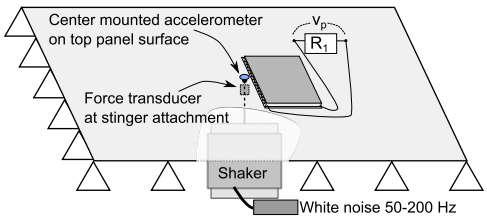

Fig. 8. Panel test schematic with the EHVA placed close to panel center.

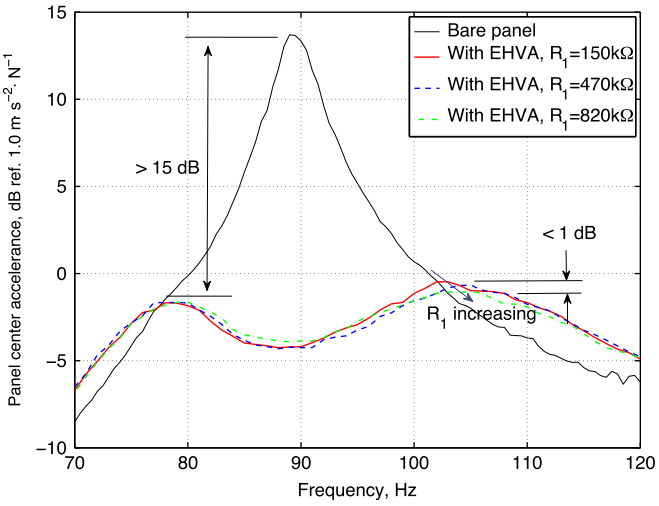

Fig. 9. Panel accelerance of the (1,1) mode before and after application of the EHVA, $\mu = 0.0102$, as R_1 is modified.

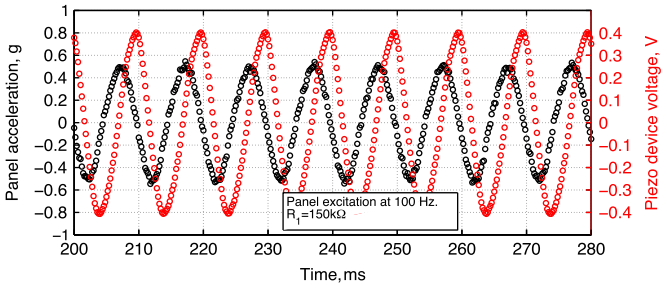

Fig. 10. Panel acceleration and EHVA electrode pair voltage output across $R_1 = 150\ \text{k}\Omega$ when the panel is excited at 100 Hz.

regarding damping induced via piezoelectric energy harvesting [9,10,12,13]. In other words, as R_1 is modified the piezoelectric spring is stiffened and damped to varying degrees, which thereafter affects how it dynamically couples to the vibrating panel.

Past piezoelectric energy harvesting studies have exploited this shunt damping effect, for instance in the simultaneous suppression of wing flutter while converting the piezoceramic harvester strain energy into electrical power [48]. In that study, 6 dB attenuation of the flow-induced vibration was achieved. In the present work, less than 1 dB additional attenuation of the split resonance around 104 Hz is achieved. However, the device *mechanically* attenuates the panel vibration by greater than 15 dB. Since a mechanically undamped vibration absorber would induce lightly damped split resonances (the dissipation being the result of host structural losses), it is observed that the much more damped split resonances induced by the EHVA in Fig. 9 at 79 and 104 Hz are the result of the mechanical damping features of the PVDF film itself and not a consequence of energy harvesting. As was noted in Section 4, the mechanical loss factor of the EHVA samples was at a minimum around 5.5% which represents an average value of mechanical loss factor for PVDF film depending on the polymer blend [49], and sets a baseline for the anticipated mechanical losses the present EHVA will induce.

Fig. 10 plots the time response of the base panel center acceleration and the EHVA electrode pair voltage response across a load resistance of $R_1 = 150\ \text{k}\Omega$ when the panel is excited only at 100 Hz. In the present configuration, maximum EHVA voltage would be measured when the device mass layer is displaced in the downward-most position of its SDOF vibration cycle, as shown in Fig. 3. Positive accelerations indicate the panel is displacing downwards.

For clarity, consider the response in Fig. 10 at the time of 210 ms. The acceleration is nearly zero (the panel is not displaced from equilibrium) and the induced voltage in the harvesting circuit is most positive (the EHVA top mass is displaced most downwards). This serves as validation for the term vibration "absorber" given that the panel displacement is nearly zero while the EHVA top mass is most displaced in its cycle. These dynamics are furthermore characteristic of 2DOF systems when the individual natural frequencies of the sub-systems are very similar [50]. Additionally, in Fig. 10 the device electrical response is observed to be very nearly linear under the present excitation amplitude. Linearity was also observed for higher levels of excitation in Ref. [51] for the present EHVA design.

Fig. 10 also indicates that for a peak acceleration of approximately 0.5 g ($4.9\ \text{m s}^{-2}$), the EHVA outputs an average electrical power of 0.560 μW. (Assuming a peak voltage of $v_p = 0.41$ V and computing average power as $P_{ave} = v_p^2/2R_1$). Though this is a small amount of electrical power compared to other energy harvester prototypes in the literature [52], the present device uses piezoelectric film for conversion of the mechanical strain to electrical potential. Piezoelectric film is substantially less electromechanically coupled than the more conventional piezoceramics of many harvester prototypes in the literature and thus yields a reduced net electrical output. From other testing including evaluation on the shaker platform, the amplitude of electrical output was observed to be readily influenced by the consistency of the etching which, as mentioned in Section 3 was carried out by hand. As a result, while some samples achieved very high electrical output despite using PVDF film (*i.e.* as opposed to highly coupled PZT materials) like sample 1 in Fig. 7(b), other samples were less promising simply due to present manufacturing limitations. Lastly, the mechanical damping of the present EHVA design is notably more dominant than the energy harvesting damping that is induced, as indicated in Fig. 9. So, while the sample used for the plate testing may have not been as accurately constructed as for instance sample 1 of Fig. 7, it may be argued that the mechanical losses of the piezoelectric film make the present EHVA design better suited to vibration control than energy harvesting.

6. Application test: EHVA on a city bus structural panel

A fundamental element in vibrational energy harvesting is the selection of sources of ambient vibration of sufficient magnitude and continuity such that energy may be consistently converted. This is one practical reason why large bridges are a typical focus: vibration due to either moving vehicular loads [53] or wind-induced vibrations [54] are regular and rarely cease entirely. Another reason why bridges are often of interest is that they are also the focus of structural health monitoring applications where power supplied by energy harvesting devices would be advantageous.

Though it might not be feasible to simultaneously attenuate bridge vibrations while converting the absorbed energy into electrical power, other common sources of vibration are much better suited for the application of an EHVA. For example, structural panels in many transportation systems (airplanes, ships, automobiles, etc.) are regularly excited in their lowest order modes, the vibration of which may itself be undesired if not also the radiation of noise from the panel due to fluid–structure interaction. In many such modern vehicles, there is a significant mass of power transmission cabling strung from the main power source (combustion engine, jet engine, etc.) through the chassis of the vehicle. It may be that vibrational energy harvesting may serve to reduce the necessity for such cabling mass and thus lighten the load carried by the engine (assuming the EHVA to be lighter than the cabling mass it replaces), making the vehicle more mobile and over greater distances.

A typical city bus is the focus for the present EHVA, Fig. 11. Within the bus is located a structural panel which is partially suspended and supported by several bolts, serving as a safety guard for passengers near to the rear door. Fig. 12 shows the panel with a shaker attachment and an accelerometer array. The panel is outlined by a green dash; some of the

Fig. 11. A city bus, the target of the EHVA application.

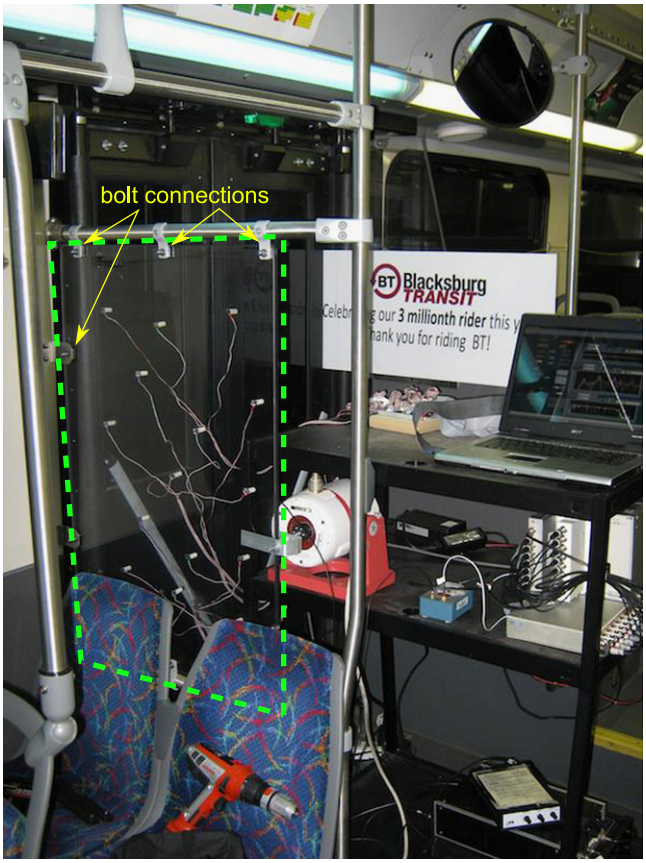

Fig. 12. Structural panel near rear door instrumented with accelerometer array and attached to shaker for testing. The panel span is indicated by the green dash lines; some mounting bolts are featured via yellow arrows. (For interpretation of the references to color in this figure caption, the reader is referred to the web version of this article.)

mounting bolts are indicated by yellow arrows. In day-to-day use, it is found that the panel, composed of an 11 mm thick piece of polycarbonate plastic, vibrates substantially due to even small road vibration input. While the bus idles, the diesel engine vibrations, transmitted through the chassis, are themselves capable of exciting the panel in its lowest modes. Though the panel is made of a highly damped plastic material, the method of securing the panel with poles directly attached to the bus chassis ensures that the amplitude of panel vibrations are significant. To prevent the vibrations from impacting the seats in front of the panel, the transit authority installed thick bumpers between the seat and the panel, which in fact result in the pair of seats vibrating along with the panel.

It is was therefore desired to develop an EHVA for the purpose of attenuating the panel vibrations as well as to show the potential for such devices to be useful sources of electrical power, for instance to reduce the necessity of power transmission cabling. After taking preliminary vibration measurements of the structural panel, it was found that the lowest natural frequencies occurred at 14, 38.5 and 44.5 Hz. Finite element (FE) modeling determined the operational deflection shapes of these frequencies. (The model was constructed using a 2D Mindlin plate eigenfrequency analysis with bolt connections modeled as point simple supports.) Fig. 13 plots the predicted mode shapes for the lowest six resonances; the mounting bolts are shown as black dots in each image.

From an energy harvesting perspective, it is desirable to apply a harvester device which exhibits a natural frequency equal to the lowest order vibrational response of the main structure. In this case, the first mode occurred at 14 Hz. From a practical perspective, it was known that constructing the present EHVA design was difficult for such low frequencies. To achieve an EHVA resonance below approximately 20 Hz, either the thickness of the corrugated piezoelectric film could be reduced or the mass of the top layer could be increased. However, in both cases laboratory experience showed that achieving natural frequencies less than 20 Hz inevitably resulted in static deformation of the spring due to mass loading; this led to a highly nonlinear elastic and electric response and typically device self-destruction for even moderate excitation levels. This represents a limitation of the present device design in achieving useful electrical output but other studies have indeed developed prototype piezoelectric harvesters having resonance frequencies below 20 Hz without detrimental nonlinearities [55]. Thus, for the present EHVA design, it was determined to target the attenuation of and energy harvesting from the second mode of the panel at 38.5 Hz which would, naturally, be the second most easily excited mode of the panel due to impulsive sources like road vibration.

An EHVA was therefore constructed with a corrugated piezoelectric film thickness of 52 μm and wavelength 25.4 mm. An analytical model [51] predicted the device would exhibit a SDOF natural frequency of approximately 39 Hz. A layer of double-sided tape was added to the bottom non-poled PVDF film sheet for secure adhesion to the bus panel. The EHVA was then applied to the panel centerline as close to the position of the second mode antinode as possible; the EHVA position is indicated by the black outline in Fig. 13. The mass ratio of the EHVA relative to the panel was measured to be $\mu = 0.0361$ or 3.61%.

The shaker connection to the panel (via a stinger and force transducer) was positioned so as to excite both the symmetric and asymmetric modes. The panel vibration before and after application of the EHVA for several load resistances is shown in Fig. 14; the untreated panel vibration is indicated by the dashed plot. The panel mode at 14 Hz is slightly attenuated and shifted in frequency slightly due to mass loading of the EHVA. At 38.5 Hz, the EHVA substantially suppresses the vibration inducing split resonances at 37 and approximately 43 Hz. The higher split resonance becomes blended into the frequency response for the third mode at 44.5 Hz, making it difficult to distinguish between the two distinct dynamics. Due to the positioning of the EHVA on a nodal line of the third mode, none of the third mode vibration is attenuated. Simply by coincidence because of the proximity in frequency of the second and third modes, there is a dramatic difference in vibration response from 41 to 44 Hz: a 23 dB difference as indicated in Fig. 14(b).

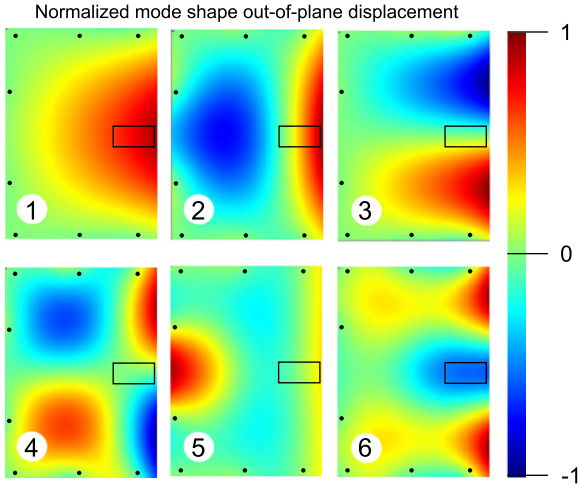

Fig. 13. Lowest six modes of bus panel predicted by FE analysis; modal number indicated in the white circle; black dots indicate the mounting bolt locations; EHVA device placement outlined in black.

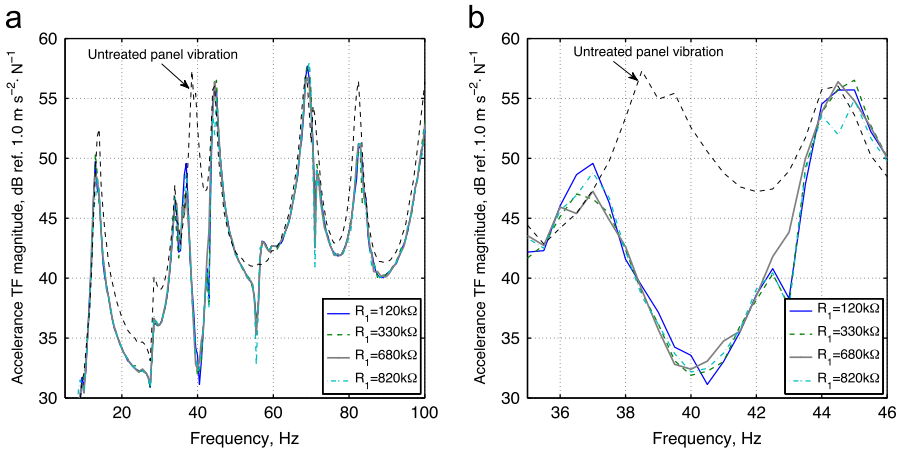

Fig. 14. Panel vibration before and after application of the EHVA for a variety of R_1: (a) full spectrum measured and (b) around the SDOF natural frequency of the EHVA (second panel mode).

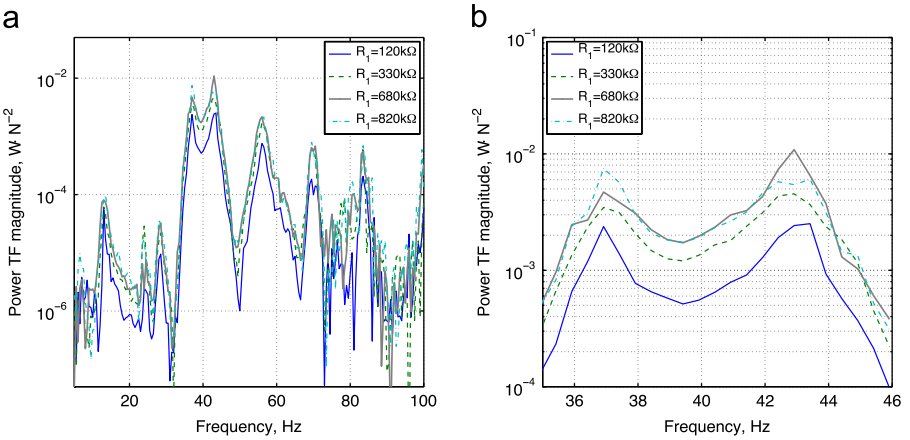

Fig. 15. Power transfer function magnitude output by the EHVA for a variety of R_1: (a) full spectrum measured and (b) around the SDOF natural frequency of the EHVA (second panel mode).

As is clearer in Fig. 14(b), changes in the load resistance are found to provide increased levels of shunt damping. Such changes appear to influence the lower and higher split resonances individually. This is difficult to determine with assurance for the higher split resonance due, again, to the close proximity of the third mode. However, for the lower split resonance at 37 Hz it is seen that a load resistance of $R_1 = 330$ or 680 kΩ provide approximately a 3 dB increase in shunt damping effects as compared with $R_1 = 120$ kΩ. But, as in the laboratory test in Section 5, the mechanical influence of the EHVA dominates in terms of achieving panel vibration attenuation.

Fig. 15 plots the power transfer function (TF) (average electrical power against the input force) for a variety of load resistances. It is clear that the EHVA outputs maximum electrical power at the frequencies of the two split resonances. Fig. 15(b) also shows that the higher split resonance occurs at 43 Hz as opposed to truly being blended into the third mode at 44.5 Hz. As in other energy harvesting studies, there may be found an optimum selection of R_1 to maximize the harvested power for the device excited near to its natural frequency [14]. Like the earlier laboratory test, due to the dynamic coupling between the device and the panel, the EHVA outputs greatest electrical power at the split resonance of 43 Hz as opposed to its original, or tuned, natural frequency of 39 Hz.

The electrical power generated for three frequencies and a variety of load resistances is plotted in Fig. 16. The maximum power TF achieved occurs at 43 Hz with a load resistance of $R_1 = 680$ kΩ: 0.0109 W N^{-2}. Therefore, the shaker then excited the panel with single frequency vibration at 43 Hz and the EHVA was attached to a load resistance of 680 kΩ. The amplitude of acceleration of the panel directly beneath the EHVA was 2.61 g (25.6 m s^{-2}). The average power was computed to be 13.6 μW (peak voltage of 4.30 V across the load resistance). From the limitations imposed by the panel modal frequencies and the design and placement of the EHVA, this is a reasonable achievement for an energy harvesting design using piezoelectric film for electromechanical conversion. Furthermore, this power output occurs simultaneously while the device suppresses the panel vibrations at the second mode by approximately 8 dB. In the absence of such design

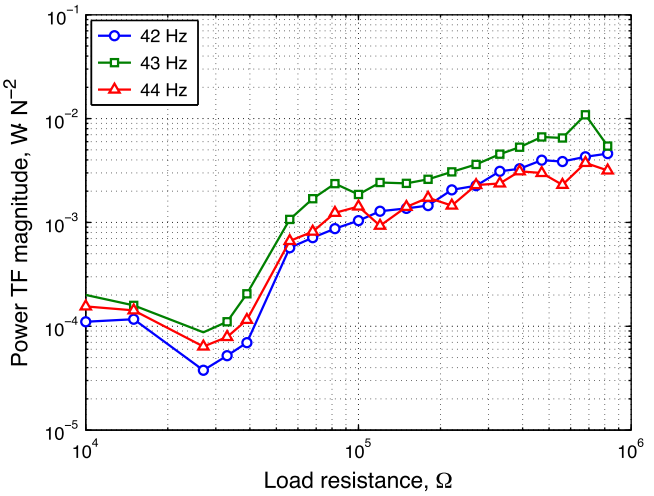

Fig. 16. Power transfer function magnitude for a variety of load resistances at 42, 43 and 44 Hz.

constraints, particularly the inability to "tune" the device for the mode at 14 Hz, it is likely that much improved performance for vibration control and energy harvesting objectives may be attained.

A final point should be made in regard to the metric of the power transfer function. For a 1D analysis of an EHVA on a main vibrating system, this TF is appropriate and yields meaningful information. Namely, this is because the main system acceleration would be directly related to the driving force by Newton's second law. Therefore, one could determine the amount of main system acceleration for convenient comparison to other harvesting metrics in the literature (often W g^{-2}). However, for distributed parameter systems, the acceleration is spatially dependent. Thus, the power TF measured earlier as 0.0109 W N^{-2} seems to suggest that for a unit force input, the device could generate 10.9 mW of power which unfortunately is not the case since the applied force must accelerate the full surface. The use of the power TF, though providing useful spectral plots indicating where maximum electrical output is achieved, is limited in benefit for distributed parameter systems. The *actual* electrical power generated during single frequency excitation is perhaps the best alternative for comparison to other results in the literature.

7. Conclusions

To date, simultaneous energy harvesting and vibration control has been pursued via several routes. Direct shunt damping effects on the harvesters themselves have been widely explored. In addition, other studies have exploited the electrical damping effect to attenuate the vibrations of the main structure to which the harvesters are applied, *e.g.* piezoelectric patches on vibrating structures. In contrast, the present study sought to exert a substantially increased mechanical influence on the host structure by designing the harvester in the style of a classical vibration absorber having an included electromechanical conversion mechanism.

The development process of the present EHVA, utilizing a circularly corrugated piezoelectric film as the distributed spring layer, was described in detail. After determination of appropriate design and manufacturing approaches, several EHVA samples were found in laboratory and field tests to be capable of significant mechanical vibration attenuation though minor shunt damping effects were observed as a result of the energy harvesting circuit connection. The measured electrical power output for these tests during single frequency excitation—0.560 μW and 13.6 μW, respectively—may be less than other harvesters in the literature, but it should be emphasized that the present EHVA achieved these results while simultaneously providing substantial attenuation of the host structural vibrations.

Were it possible to decrease the piezoelectric film spring layer mechanical damping it is likely that greater electrical output would be achieved since the EHVA would be more resonant. At the same time, such a reduction in mechanical damping might inhibit the EHVA vibration attenuation capability depending on whether an increased shunt damping effect is consequently induced. Nevertheless, the present study showed an example of vibration control concern which may be alleviated using a device that supplies significant mechanical attenuation to meet the control problem while simultaneously converts a portion of the absorbed energy into electrical power.

Acknowledgments

The author would like to thank Blacksburg Transit (BT)—specifically Tim Witten, Aneil Samuel, Chris Stoynev and Ken Tucker—for the freedom and flexibility with which to conduct the tests onboard the bus.

References

[1] N.E. duToit, B.L. Wardle, S.-G. Kim, Design considerations for mems-scale piezoelectric mechanical vibration energy harvesters, Integrated Ferroelectrics 71 (2005) 121–160.
[2] N.G. Elvin, N. Lajnef, A.A. Elvin, Feasibility of structural monitoring with vibration powered sensors, Smart Mater. Struct. 15 (2006) 977–986.
[3] S. Priya, D.J. Inman (Eds.), Energy Harvesting Technologies, first ed. Springer, New York, NY, 2009.
[4] E.K. Reilly, L. Miller, R. Fain, P.K. Wright, A study of ambient vibrations for piezoelectric energy scavenging, in: POWERMEMS: International Workshop on Micro and Nanotechnology for Power Generation and Energy Conversion Applications, Washington, DC, 2009, pp. 312–315.
[5] S. Roundy, On the effectiveness of vibration-based energy harvesting, J. Intell. Mater. Syst. Struct. 16 (2005) 809–823.
[6] E. Lefeuvre, A. Badel, C. Richard, L. Petit, D. Guyomar, A comparison between several vibration-powered piezoelectric generators for standalone systems, Sensors Actuators A 126 (2006) 405–416.
[7] S.P. Beeby, R.N. Torah, M.J. Tudor, P. Glynne-Jones, T. O'Donnell, C.R. Saha, S. Roy, A micro electromagnetic generator for vibration energy harvesting, J. Micromech. Microeng. 17 (2007) 1257–1265.
[8] A. Erturk, D.J. Inman, An experimentally validated bimorph cantilever model for piezoelectric energy harvesting from base excitations, Smart Mater. Struct. 18 (2) (2009) 025009.
[9] R.L. Forward, Electronic damping of vibrations in optical structures, J. Appl. Opt. 18 (5) (1970) 690–697.
[10] N.W. Hagood, A. von Flotow, Damping of structural vibrations with piezoelectric materials and passive electrical networks, J. Sound Vib. 146 (2) (1991) 243–268.
[11] C.L. Davis, G.A. Lesieutre, A modal strain energy approach to the prediction of resistively shunted piezoceramic damping, J. Sound Vib. 184 (1) (1995) 129–139.
[12] G.A. Lesieutre, Vibration damping and control using shunted piezoelectric materials, Shock Vib. Dig. 30 (3) (1998) 187–195.
[13] G.A. Lesieutre, G.K. Ottman, H.F. Hofmann, Damping as a result of piezoelectric energy harvesting, J. Sound Vib. 269 (2004) 991–1001.
[14] Y. Liao, H.A. Sodano, Structural effects and energy conversion efficiency of power harvesting, J. Intell. Mater. Syst. Struct. 20 (2009) 505–514.
[15] N.G. Stephen, On energy harvesting from ambient vibration, J. Sound Vib. 293 (2006) 409–425.
[16] S.P. Beeby, M.J. Tudor, N.M. White, Energy harvesting vibration sources for microsystems applications, Meas. Sci. Technol. 17 (2006) R175–R195.
[17] B.P. Mann, N.D. Sims, On the performance and resonant frequency of electromagnetic induction energy harvesters, J. Sound Vib. 329 (2010) 1348–1361.
[18] A. Erturk, J.M. Renno, D.J. Inman, Modeling of piezoelectric energy harvesting from an l-shaped beam-mass structure with an application to uavs, J. Intell. Mater. Syst. Struct. 20 (2009) 529–544.
[19] O. Aldraihem, A. Baz, Energy harvester with a dynamic magnifier, J. Intell. Mater. Syst. Struct. 22 (2011) 521–530.
[20] W. Zhou, G.R. Penamalli, L. Zuo, An efficient vibration energy harvester with a multi-mode dynamic magnifier, Smart Mater. Struct. 21 (2012) 015014.
[21] A. Aladwani, M. Arafa, O. Aldraihem, A. Baz, Cantilevered piezoelectric energy harvester with a dynamic magnifier, J. Vib. Acoust. 134 (2012) 031004.
[22] X. Tang, L. Zuo, Enhanced vibration energy harvesting using dual-mass systems, J. Sound Vib. 330 (21) (2011) 5199–5209.
[23] X. Tang, L. Zuo, Vibration energy harvesting from random force and motion excitations, Smart Mater. Struct. 21 (2012) 075025.
[24] J.T. Scruggs, Multi-objective optimization of regenerative damping systems in vibrating structures, in: American Control Conference, 2007. ACC '07, 2007, pp. 2672–2677. http://dx.doi.org/10.1109/ACC.2007.4282730.
[25] R.L. Harne, Theoretical investigations of energy harvesting efficiency from structural vibrations using piezoelectric and electromagnetic oscillators, J. Acoust. Soc. Am. 132 (1) (2012) 162–172.
[26] S.C. Huang, D.J. Inman, E.M. Austin, Some design considerations for active and passive constrained layer damping treatments, Smart Mater. Struct. 5 (1996) 301–313.
[27] A. Baz, J. Ro, Vibration control of plates with active constrained layer damping, Smart Mater. Struct. 5 (1996) 272–280.
[28] J.C. Snowdon, Vibration of simply supported rectangular and square plates to which lumped masses and dynamic vibration absorbers are attached, J. Acoust. Soc. Am. 57 (3) (1975) 646–654.
[29] G. Maidanik, K.J. Becker, Noise control of a master harmonic oscillator coupled to a set of satellite harmonic oscillators, J. Acoust. Soc. Am. 104 (5) (1998) 2628–2637.
[30] I.M. Koç, A. Carcaterra, Z. Xu, A. Akay, Energy sinks: vibration absorption by an optimal set of undamped oscillators, J. Acoust. Soc. Am. 118 (5) (2005) 3031–3042.
[31] R.J. Nagem, I. Veljkovic, G. Sandri, Vibration damping by a continuous distribution of undamped oscillators, J. Sound Vib. 207 (3) (1997) 429–434.
[32] C.R. Fuller, P. Cambou, An active–passive distributed vibration absorber for vibration and sound radiation control, J. Acoust. Soc. Am. 104 (3) (1998) 1851.
[33] K. Idrisi, M.E. Johnson, D. Theurich, J.P. Carneal, A study on the characteristic behavior of mass inclusions added to a poro-elastic layer, J. Sound Vib. 329 (2010) 4136–4148.
[34] R.L. Harne, C.R. Fuller, Modeling of a distributed device for simultaneous reactive vibration suppression and energy harvesting, J. Intell. Mater. Syst. Struct. 23 (6) (2012) 655–664.
[35] F. Charette, C. Guigou, A. Berry, Development of volume velocity sensors for plates using pvdf film, in: Active 95, 1995, pp. 241–252.
[36] J. Pan, C. Hansen, D. Bies, Active control of noise transmission through a panel into a cavity: I, analytical study, J. Acoust. Soc. Am. 87 (1990) 2098–2108.
[37] H. Yu, K.W. Wang, Piezoelectric networks for vibration suppression of mistuned bladed disks, J. Vib. Acoust. 129 (2007) 559–566.
[38] C.A. Gentry, C. Guigou, C.R. Fuller, Smart foam for applications in passive–active noise radiation control, J. Acoust. Soc. Am. 101 (4) (1997) 1771–1778.
[39] C. Guigou, C.R. Fuller, Control of aircraft interior broadband noise with foam–pvdf smart skin, J. Sound Vib. 220 (3) (1999) 541–557.
[40] P. Leroy, N. Atalla, A. Berry, Three dimensional finite element modeling of smart foam, J. Acoust. Soc. Am. 126 (6) (2009) 2873–2885.
[41] A. Kundu, A. Berry, Active control of transmission loss with smart foams, J. Acoust. Soc. Am. 129 (2) (2011) 726–740.
[42] P. Marcotte, C.R. Fuller, P. Cambou, Control of the noise radiated by a plate using a distributed active vibration absorber (dava), in: Active 99, Proceedings of the International Symposium on Active Control of Sound and Vibration, Fort Lauderdale, FL, USA, 1999, pp. 447–456.
[43] G.C. Tibbetts, Transducer having piezoelectric film arranged with alternating curvatures, U.S. Patent #4,056,742, 1977.
[44] A. Erturk, P.A. Tarazaga, J.R. Farmer, D.J. Inman, Effect of strain nodes and electrode configuration on piezoelectric energy harvesting from cantilevered beams, J. Vib. Acoust. 131 (1) (2009).
[45] COMSOL, COMSOL Multiphysics User's Guide, COMSOL AB., Burlington, MA, October 2007.
[46] R.L. Harne, C.R. Fuller, Modeling of a passive distributed vibration control device using a superposition technique, J. Sound Vib. 331 (8) (2012) 1859–1869.
[47] J.P. Den Hartog, Mechanical Vibrations, fourth ed. Dover Publications, New York, NY, 1985.
[48] C. De Marqui Jr., A. Erturk, D.J. Inman, Piezoaeroelastic modeling and analysis of a generator wing with continuous and segmented electrodes, J. Intell. Mater. Syst. Struct. 21 (2010) 983–993.
[49] K. Koga, H. Ohigashi, Piezoelectricity and related properties of vinylidene fluoride and trifluoroethylene copolymers, J. Appl. Phys. 59 (6) (1986) 2142–2150.
[50] D.J. Inman, Engineering Vibration, second ed. Prentice-Hall, Upper Saddle River, NJ, 2001.
[51] R.L. Harne, Concurrent attenuation of and energy harvesting from surface vibrations: experimental verification and model validation, Smart Mater. Struct. 21 (2012) 035016.

[52] S.R. Anton, H.A. Sodano, A review of power harvesting using piezoelectric materials (2003–2006), Smart Mater. Struct. 16 (2007) R1–R21.
[53] A. Erturk, Piezoelectric energy harvesting for civil infrastructure system applications: moving loads and surface train fluctuations, J. Intell. Mater. Syst. Struct. 22 (17) (2011) 1959–1973.
[54] Y. Fujino, Vibration, control and monitoring of long-span bridges—recent research, developments and practice in Japan, J. Constr. Steel Res. 58 (2002) 71–97.
[55] M.A. Karami, D.J. Inman, Analytical modeling and experimental verification of the vibrations of the zigzag microstructure for energy harvesting, J. Vib. Acoust. 133 (2011) 011002.